



Heat flow estimated from BSR and IODP borehole data: Implication of recent uplift and erosion of the imbricate thrust zone in the Nankai Trough off Kumano

Masataka Kinoshita

*IFREE, Japan Agency for Marine–Earth Science and Technology, Yokosuka, Kanagawa 237-0061,
Japan (masa@jamstec.go.jp)*

Gregory F. Moore

*Department of Geology and Geophysics, University of Hawai‘i at Mānoa, Honolulu, Hawaii 96822,
USA*

*IFREE, Japan Agency for Marine–Earth Science and Technology, Yokosuka, Kanagawa 237-0061,
Japan*

Yukari N. Kido

*CDEX, Japan Agency for Marine–Earth Science and Technology, Yokohama, Kanagawa 236-0001,
Japan*

[1] Heat flow values were estimated in the Nankai Trough fore-arc slope region off Kii Peninsula from the Bottom-Simulating Reflector (BSR) and other data obtained during IODP Expeditions 315 and 316. The heat flow has an uncertainty of ~20% mainly due to ambiguities in the temperature estimate at the BSR and uncertainties on the thermal conductivity. BSRs occur intermittently in the Imbricate Thrust Zone (ITZ). They are significantly shallower below anticlines, designated “Anticlinal High Zone” (AHZ), than in the adjacent synclines (“Basal Low Zone” (BLZ)). The heat flow in the BLZ (55–65 mW/m²) is consistent with the regional heat flow trend. The shallow BSR in the AHZ produces an apparent high heat flow anomaly of 70–90 mW/m², and discontinuities are observed across thrust faults. The most likely cause is the transient effect of thrust faulting followed by erosion on the hanging wall side. A one-dimensional time-dependent numerical model, with latent heat for hydrate and gas transition considered, indicates that the relaxation time for the BSR to reequilibrate after such a disturbance is ~10 kyr. Although the possibility that the shallow BSR is a remnant base of hydrate stability zone cannot be ruled out, if the shortening has occurred in the recent 10 kyr the convergent rate at the ITZ would be ~30 m/kyr, which is much larger than the recent horizontal shortening across the megasplay fault, and could even exceed the portion of the plate convergence than that accommodated at the frontal thrust.

Components: 8600 words, 12 figures, 1 table.

Keywords: BSR; IODP; NanTroSEIZE; heat flow; imbricate thrust; methane hydrate.

Index Terms: 3015 Marine Geology and Geophysics: Heat flow (benthic).

Received 11 March 2011; **Revised** 14 July 2011; **Accepted** 14 July 2011; **Published** 21 September 2011.

Kinoshita, M., G. F. Moore, and Y. N. Kido (2011), Heat flow estimated from BSR and IODP borehole data: Implication of recent uplift and erosion of the imbricate thrust zone in the Nankai Trough off Kumano, *Geochem. Geophys. Geosyst.*, 12, Q0AD18, doi:10.1029/2011GC003609.

Theme: Mechanics, Deformation, and Hydrologic Processes at Subduction Complexes,
With Emphasis on the Nankai Trough Seismogenic Zone Experiment (NanTro-
SEIZE) Drilling Transect

Guest Editors: D. Saffer, P. Henry, H. Tobin, and F. Chester

1. Introduction

[2] The Nankai Trough fore-arc system (Figure 1) forms an active subduction complex with a seismogenic zone of great earthquakes and tsunamis. Along the Nankai Trough, the Philippine Sea Plate, with its age range of 15–25 Ma [Okino *et al.*, 1994], is subducting beneath the Japan island arc at ~5.8 cm/year [DeMets *et al.*, 2010]. Similar to other subduction zones in the world located close to the continent or island arcs, the floor of the trough is filled with thick turbidite sediment, which is offscraped to form an accretionary prism landward of the trough. In the Kumano transect (Figure 2), however, the frontal imbrications appear to have ceased until recently and the frontal thrust extends 6 km landward [Moore *et al.*, 2009; Sreaton *et al.*, 2009b]. In the imbricate thrust zone (ITZ; Figure 2), progressive deformation due to horizontal tectonic compression has formed a series of thrust faults beneath the fore-arc slopes. Between the ITZ and décollement is a low velocity zone (LVZ; Figure 2) [Park *et al.*, 2010].

[3] The thermal structure of an accretionary wedge complex provides one of the critical keys to understand the mechanism for subduction zone earthquakes. Heat flow data provide an essential constraint toward more reliable thermal modeling. In the Nankai Trough region, heat flow data have been obtained through probe measurements [Kinoshita *et al.*, 2008]. However, it is difficult to obtain reliable heat flow values in the fore-arc slope region because of rugged topography, rapid sedimentation/erosion due to landslides [Strasser *et al.*, 2009, 2011], and temperature variations in the water column that disturbs subbottom temperatures.

[4] An alternative way to determine heat flow is to use the depth to bottom-simulating reflectors (BSRs), which define a boundary between the hydrate-rich formation above and a gas-bearing layer below [e.g., Shipley *et al.*, 1979; White, 1979]. The occurrence of gas hydrate is controlled by temperature, pressure and composition of gas and water [e.g., Kvenvolden, 1993]. Using this relation-

ship, the first developments of this method were conducted in the Nankai prism [Yamano *et al.*, 1982; Hyndman *et al.*, 1992]. In deep sea areas, BSRs are located a few hundreds of meters below the seafloor. Thus short wavelength variations are filtered out and regionally averaged heat flow values can be obtained. Martin *et al.* [2004] used 3D seismic reflection data in the eastern Nankai Trough to calculate heat flow from the BSR, and demonstrated that the heat flow anomalies can be best explained by active erosion and sedimentation on the fore-arc slope.

[5] BSRs are mostly identified in continental margins. They are identified as reflections that are parallel to subparallel to the seafloor bathymetry. The polarity of reflected seismic wave is reversed to that from the seafloor, indicating that a lower velocity layer underlies higher velocity sediment. For example, the velocity structure of the sediments and the precise depth of the BSR in Blake Ridge were determined with vertical seismic reflection profiles conducted during ODP Leg 164. Holbrook *et al.* [1996] report that the velocity of sediments overlying the BSR at ODP Site 997 is ~1850 m/s whereas velocities of ~1400 m/s were measured beneath the BSR, and indicated the presence of free gas.

[6] To form an identifiable BSR in the seismic profiles, a strong contrast in the acoustic impedance between above and below BSR is necessary, which is attributed to the existence of a hydrate zone above, but more significantly, to the presence of free gas below the base of gas hydrate stability (BGHS) interface [e.g., Singh *et al.*, 1993].

[7] Through numerical simulation of mass balance equations, Davie and Buffet [2001] showed that in situ biogenic methane production can explain an observed hydrate distribution in the Blake Ridge, and that hydrate is unlikely to occupy more than 7% of the pore volume in a passive margin where no deeper sources of fluid is supplied. Hyndman and Davis [1992] found that BSRs, while rare in normal-setting deep sea basins, are common in coarse clastic accretionary sedimentary wedges.

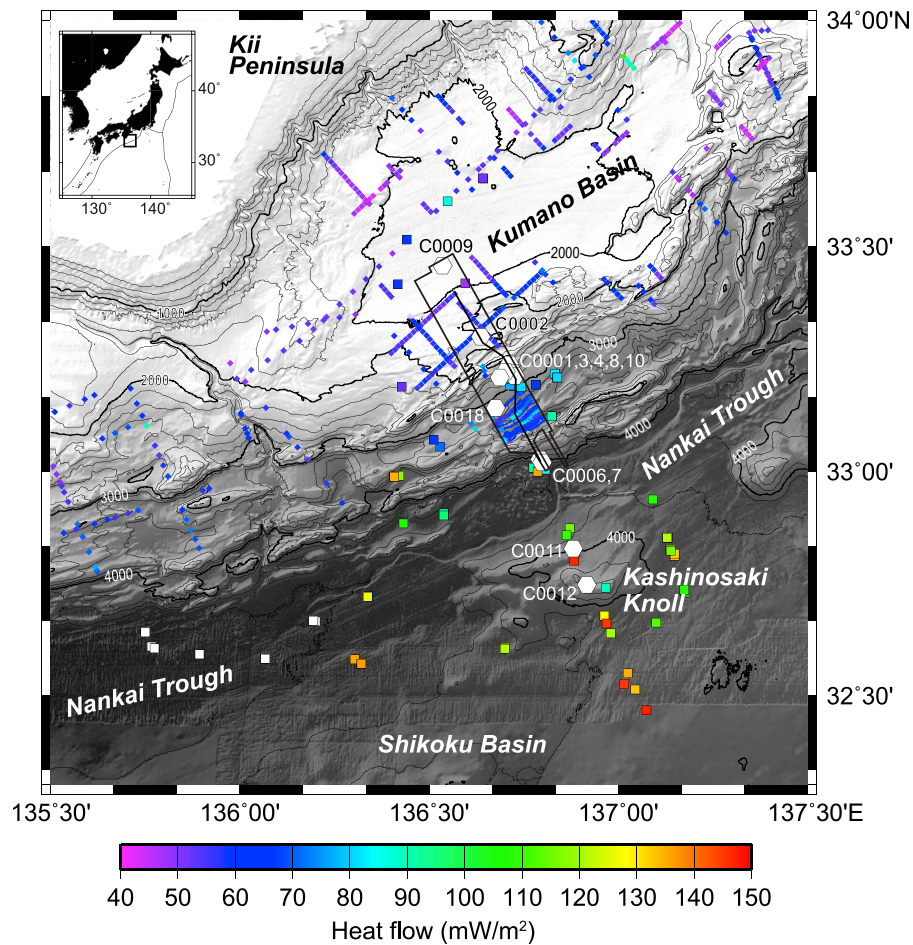


Figure 1. Index map showing bathymetry and heat flow distribution. Box is the area covered by the 3-D seismic survey, solid line is the composite seismic line in Figure 2, and open hexagons are the locations of IODP drill sites.

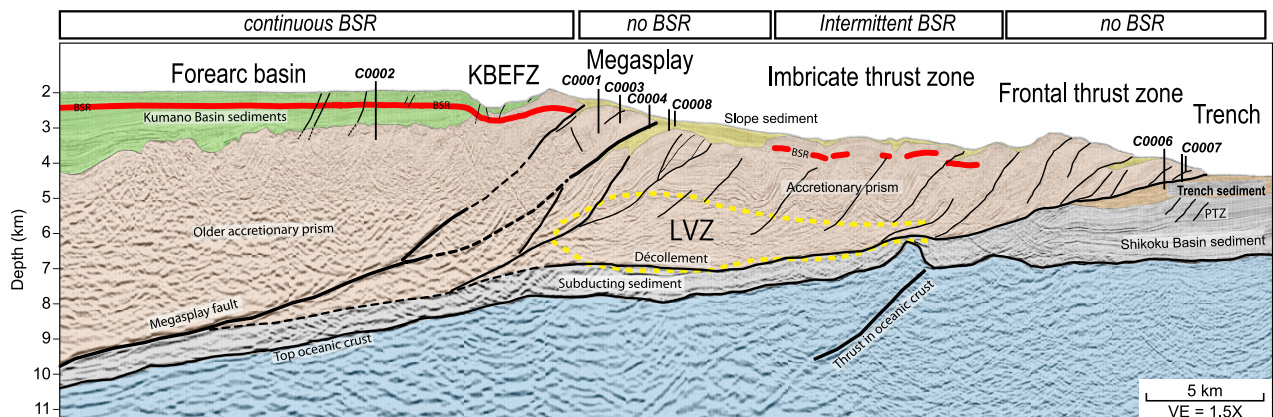


Figure 2. Composite Inline profile of the 3D seismic volume across NanTroSEIZE drill sites (modified from Moore et al. [2009]). The low-velocity zone (LVZ [Park et al., 2010]) is shown by the yellow dashed curve.

[8] In accretionary wedges, some mechanism to collect a large enough volume of gas is required, such as upward fluid migration or hydrate recycling by dissociation of hydrate [e.g., *Kvenvolden, 1993*]. *Ashi et al.* [2002] pointed out that strong BSRs are attained by upward migration of fluid or gas, sedimentation, uplift and tectonic stacking. *Haacke et al.* [2007] show that free gas accumulation beneath the gas hydrate stability zone (GHSZ) is dominated by hydrate recycling in active areas with rapid rates of upward fluid flow and seabed uplift, such as in subduction zone accretionary wedges.

[9] Assuming the hydrate phase is Type I pure methane hydrate, the depth to the BGHS is primarily constrained by the formation temperature and pressure. Then BSRs can be interpreted as a proxy for environmental/tectonic disturbances, such as climate or sea level changes, landslides, uplift/subsidence, sedimentation/erosion [e.g., *Kvenvolden, 1993*], or fluid flow along permeable pathways such as fault zones [e.g., *Hyndman and Davis, 1992*]. On the other hand, *Ruppel* [1997] showed that the occurrence of the Blake Ridge BSR at an anomalously shallow depth (or that the temperature at BSR estimated from borehole measurements is shifted by -2°C or more) cannot be explained by realistic combinations of sea level rise and bottom water temperature increase, and suggested that the properties of sediments or pore fluids (e.g., capillary forces in clay-rich sediment) may inhibit the stability of gas hydrate. Through a thermodynamical calculation for hydrate formation, *Henry et al.* [1999] argued that this temperature anomaly requires additional factors such that the system is not in thermodynamic equilibrium but is controlled by the kinetics of hydrate nucleation and growth.

[10] The multidisciplinary Nankai Trough Seismogenic Zone Experiment (NanTroSEIZE) are being carried out across the accretionary prism in the Nankai Trough in order to understand the mechanism of great earthquakes and tsunamis along subduction zones [*Tobin and Kinoshita, 2006; Kinoshita et al., 2009*]. In 2006, a 3-D seismic reflection survey was conducted off Kumano in preparation for Integrated Ocean Drilling Program (IODP) drilling [*Moore et al., 2007, 2009*]. High-resolution images in the shallower portion enable detection of BSRs beneath the fore-arc slope, as well as in the Kumano fore-arc basin area. BSRs had barely been identified in this region through previous 2D seismic surveys [e.g., *Park et al., 2002*]. The deformation structures and depositional/erosional features are also imaged in detail. *Bangs et al.* [2010] noticed the existence of a paleo-BSR above the present BSR near a V-shaped

depression on the southern edge of the Kumano Basin. They attribute the paleo-BSR to the erosion that produced a V-shaped ‘notch’ structure (KBEFZ in Figure 2).

[11] Since 2007, a suite of IODP expeditions has been carried out within the 3-D seismic survey area. So far 13 sites have been drilled from the Shikoku Basin to the Kumano fore-arc Basin (Figure 1), and physical properties were systematically obtained both by in situ downhole logging and by core measurements onboard.

[12] In this paper, we report the heat flow values estimated from the depths of BSRs in the imbricate thrust zone (ITZ [*Moore et al., 2009*]) beneath the fore-arc slope. To estimate the heat flow we used the thermal conductivity [*Harris et al., 2011*] and P wave velocity data measured on core samples or logged in the nearby boreholes drilled during IODP Expeditions 315/316 [*Ashi et al., 2009; Sreaton et al., 2009a*]. Based on the spatial distribution of BSR depths, we propose a model to explain some local BSR depth anomalies in the ITZ by considering the transient thermal effect due to faulting.

2. Heat Flow Estimation From BSR

[13] Heat flow can be estimated as the product of vertical temperature gradient and the thermal conductivity of the formation. The most direct method is to penetrate a geothermal probe into the sediment, in which 6–8 thermistors are mounted along a 4–6 m long lance [e.g., *Hyndman et al., 1979*]. This provides the value of the temperature gradient through the seafloor. During drilling operations, temperature measurements made ahead of the drilling bit can provide heat flow values down to a depth of a few hundred meters below the seafloor [e.g., *Davis et al., 1997*].

[14] The other method used in this study is based on BSR depth, first introduced by *Yamano et al.* [1982]. This method assumes that the location of the BSR corresponds to the *present* base of hydrate stability zone (BHSZ). Temperature gradients can be calculated from the interval between the seafloor and BSR and temperatures on the seafloor and at the BSR.

2.1. BSR Horizon Picking

[15] We first used the prestack time migration (PSTM) volume data [*Moore et al., 2007*] to identify BSR horizons. Picks were made manually by eye, using commercial software “Paradigm 3D Canvas,” on every 10 inline profiles from IL2130 to IL2750, in the fore-arc slope region between crossline ~XL4020 and

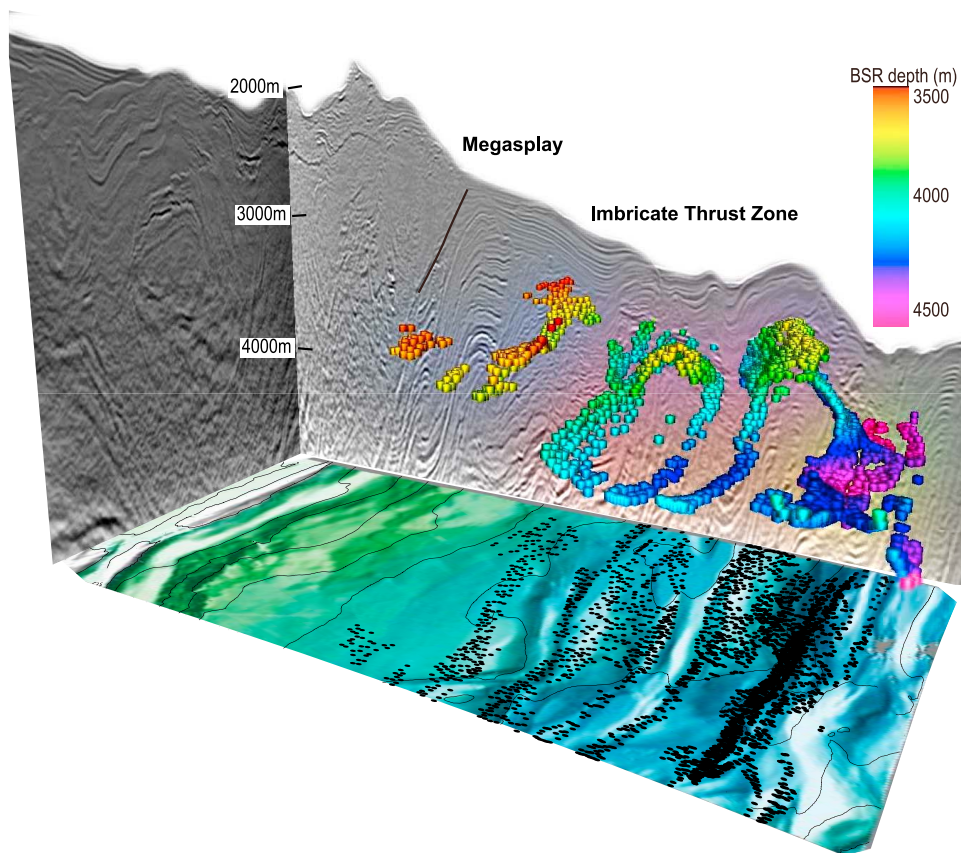


Figure 3. Three-dimensional view of BSR distribution in the fore-arc slope region drawn against the 3D PSDM profile. Colors correspond to the depth of BSR from mean sea surface. The bathymetry is shown at the bottom, where black dots are the location of BSRs.

~XL4900. Criteria for recognizing the BSR include the polarity of first arrival being opposite to that from the seafloor, and that the reflector is nearly parallel to the seafloor at ~400 msec (two-way traveltime).

[16] The time domain records are probably more accurate for picking horizons than the depth-domain records because the wavelength remains constant throughout the vertical direction. However, we had problems with picking BSR horizons which are parallel to strata.

[17] Because the BSR in images from the prestack depth migrated (PSDM) volume is much clearer than in the time domain images [Moore *et al.*, 2009], our final picks were modified using the PSDM volume, at every 5 to 10 inlines between crosslines 4000 to 4900. The PSDM data volume has spacing

of 12.5 m between crosslines and 18.75 m between inlines, thus establishing the spatial resolution for the BSR at 12.5 m in the inline direction (SE to NW) and 18.75 m in the crossline direction (SW to NE). We could identify more horizons in the PSDM data with fewer ambiguities such as BSRs parallel to the strata below anticlines.

[18] Our interpretation shows that the distribution of the BSR in the fore-arc slope region is limited to the region between the footwall of the megasplay and the uplift zone near the accretionary prism toe (Figures 3–5). Also, on a more localized scale, BSRs seem to appear mostly on the rim of anticlines, obliquely crossing anticline-forming strata, as shown in Figure 4 around crosslines 4400, 4500 and between crosslines 4600 and 4700.

Figure 4. Prestack depth migration cross section view of 3D seismic volumes along inlines (a) 2160, (b) 2230, (c) 2450, (d) 2575, and (e) 2747. BSR horizons are indicated by triangles. The double BSRs are recognized on inline (IL) 2747 between crosslines (XL) 4350 and 4500. Black dashed lines show interpreted faults.

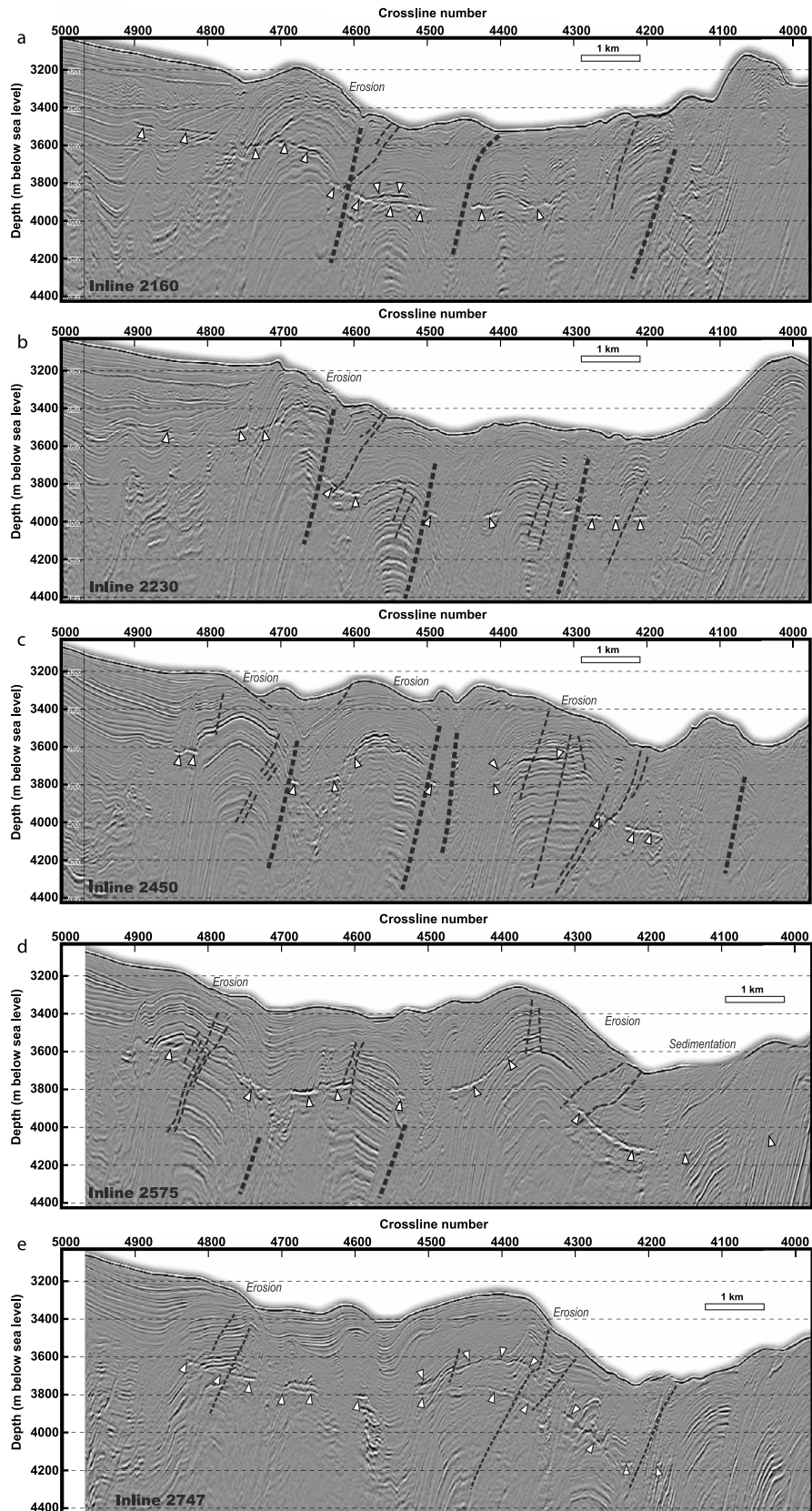


Figure 4

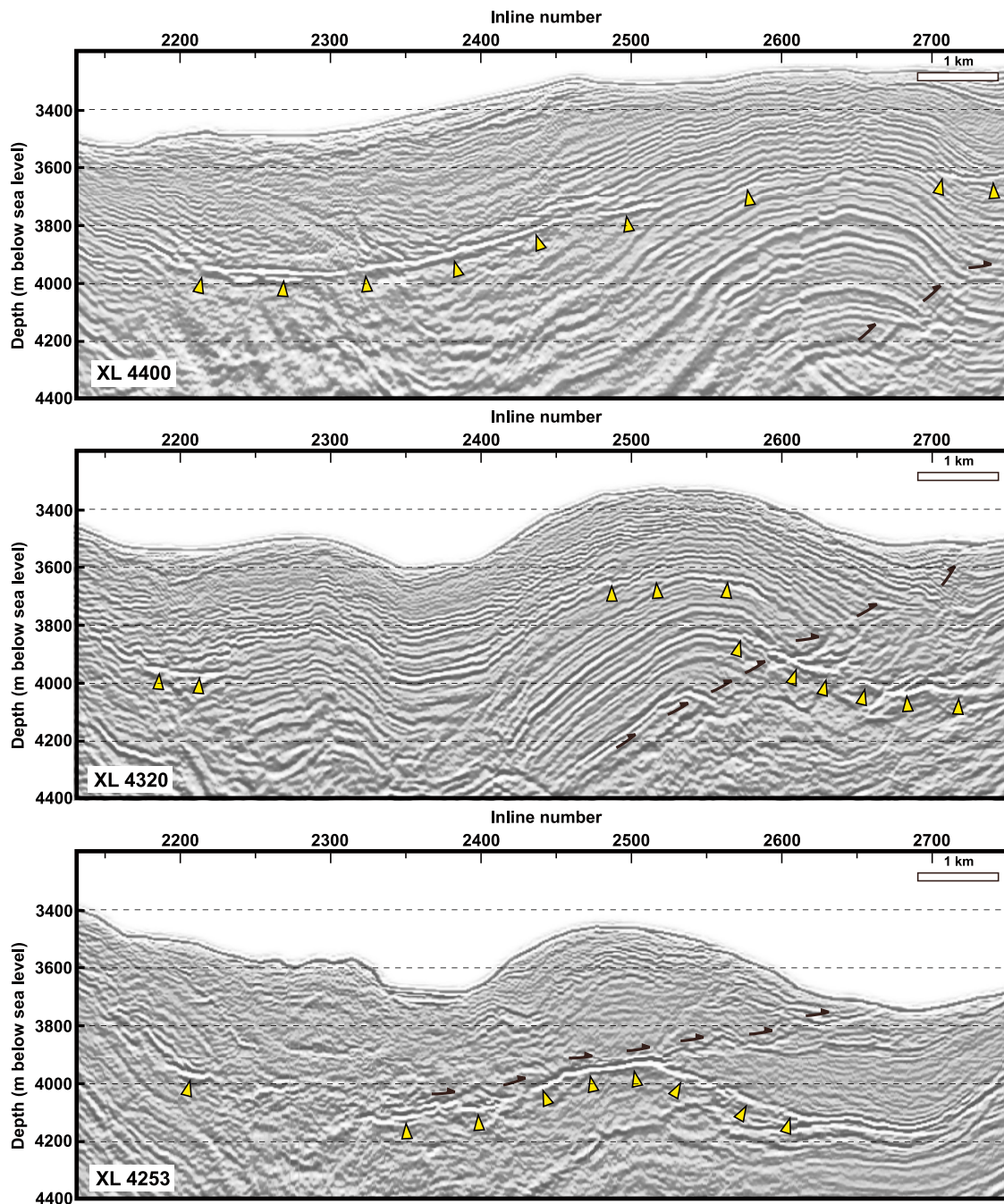


Figure 5. PSDM cross section view of 3D seismic volume along crosslines 4253, 4320 and 4400. BSR horizons are indicated by triangles. Black arrows show interpreted faults.

2.2. Uncertainty Due to Errors in the Velocity Model

[19] To assess the uncertainty in the estimates of depth to BSR, P wave velocities (V_p) were compared at drill sites C0001/C0004/C0006, between log velocities obtained by the Logging-While-Drilling (LWD) sonic tool during IODP Expedition 314 [Kinoshita *et al.*, 2009] and the interval velocity

model obtained from several iterations of 3D pre-stack depth migration analysis combined with 3D horizon-based tomography (Figure 6).

[20] Velocities basically match to one another in the shallow portion above the BSRs, but at Site C0004 (shallow megasplay), the LWD velocity is higher than the interval velocity by up to 200 m/s. To assess how the BSR depth is sensitive to the velocity

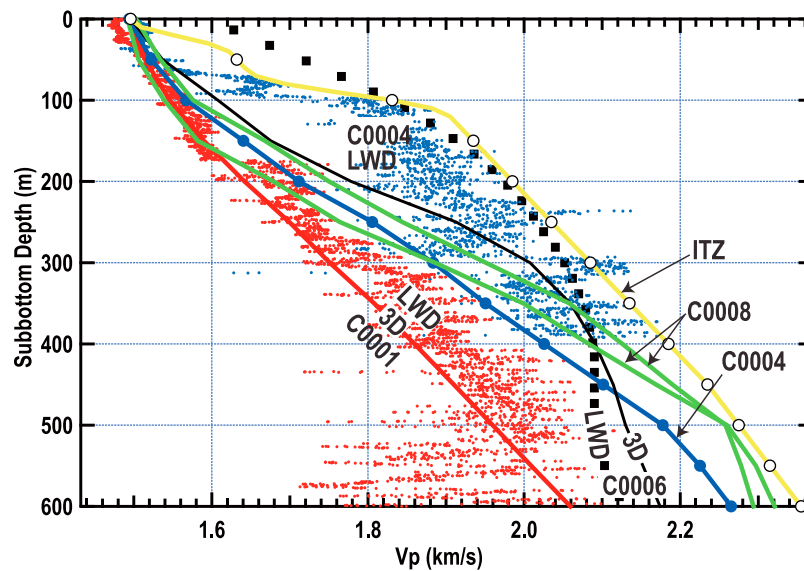


Figure 6. P wave velocity versus subbottom depth at drill sites C0001 (red), C0004 (blue), C0006 (black), and C0008 (green). Dots are velocity obtained by LWD, and curves are the interval velocity model used in 3D seismic data. Yellow curve with white circles represents the interval velocity profile in the imbricate thrust zone (ITZ).

model, we compared the depth corresponding to 400 msec (TWT) using LWD-based and interval velocity models by simply integrating the velocity from 0 to 400 msec. Their difference ranges from 2 m at Site C0001 to 25 m at Site C0006, and at all sites the interval velocity model yields deeper depths than with the LWD velocity model.

[21] Such uncertainties in the BSR depth lead to uncertainties in temperature gradient (and thus heat flow estimates). The heat flow values would change by 6% for 25 m difference and 0.5% for 2 m difference.

[22] *Tobin et al.* [2009] showed that the depth at the base of the methane hydrate layer at Site C0002 (at 400 m below the seafloor) coincides well with the BSR depth in the 3D seismic volume data. It gives us confidence about the accuracy of the BSR depth estimated in this study. We conclude that the uncertainty in heat flow due to uncertainty in V_p profiles is at most 5%.

2.3. Uncertainty Due to Resolution Limit in the Seismic Data

[23] Resolution of the seismic data is defined as one fourth of the wavelength of the data. *Moore et al.* [2009] calculated the resolution of 3D seismic data as 5–7 m near the seafloor and 10–20 m for the deepest sediment with $V_p = 2000$ – 2400 m/s. In this study, we assess that the depth resolution (and thus

the uncertainty in BSR depth) is ~ 10 m. This corresponds to a heat flow uncertainty of 1–2 mW/m^2 .

2.4. Smoothing of Bathymetry

[24] *Blackwell et al.* [1980] showed that the topographic effect on subsurface temperature field is attenuated in the form:

$$T(z) = T_0 \exp\left(-2\pi k \frac{z}{\lambda}\right),$$

where z is the depth below the seafloor, k is the wave number of topographic undulation (and thus the spatial temperature variation at a horizontal plane near the seafloor), and λ is the maximum wavelength of the topographic undulation. Thus, topographic relief whose wavelength is shorter than $2\pi z$ does not affect the temperature at depth z .

[25] For this area where the BSR depth is ~ 400 m, bathymetry was smoothed by applying a Gaussian filter to the 2D bathymetry. The cutoff wavelength is 1 km (2σ), at which wavelength the surface temperature variation is attenuated to $\sim 10\%$ around the BSR depth. This filtered bathymetry is used to calculate the smoothed subbottom depth to BSR, which is then used to calculate the temperature gradient.

[26] *Martin et al.* [2004] applied similar smoothing to the BSR. In this study, however, we did not apply smoothing to the picked BSR data, because any

short-wavelength variation in the BSR is attributed to a local origin and should not be filtered out.

2.5. Temperature and Pressure at BSR Horizon

[27] The temperature at the BSR is estimated from the P-T curve for hydrate stability based on laboratory data. There are numerous papers describing the P-T conditions for methane hydrates [e.g., *Dickens and Quinby-Hunt*, 1994; *Hyndman et al.*, 1992; *Grevenmeyer and Villinger*, 2001; *Maekawa et al.*, 1995]. They are basically identical at 30–40 MPa, except for *Dickens and Quinby-Hunt* [1994], which is applicable to 2.75–10 MPa. In this study we use the relationship by *Maekawa et al.* [1995] for the dissociation of seawater with 3.5 wt% NaCl solution. Low salinity pore fluid of about 20‰ at the BSR rather than the normal 35‰ salinity of seawater could result in a heat flow error of about 6% [*He et al.*, 2007].

[28] *Grevenmeyer and Villinger* [2001] pointed out that the temperature at BSR depth can vary by 20% due to capillary forces, chemical impurities or non-equilibrium conditions, if calibration by heat probe measurements is not available.

[29] The pore pressure at the BSR should be between lithostatic (upper bound) and hydrostatic (lower bound) states, depending on the hydrological condition between the seafloor and BSR. *He et al.* [2007] suggested that the pore pressure is more likely in a hydrostatic state down to BSR depth, because it is not deep enough to cause overpressures. *Martin et al.* [2004] also assume a hydrostatic pore pressure for temperature estimation at the BSR in the eastern Nankai Trough, because the slopes of an accretionary wedge cannot be maintained under overpressure conditions and because the temperature measured at a nearby well supports a hydrostatic condition above the BSR. *Ashi et al.* [2002] assume an intermediate density of 1.5 g/cm³ in the sediment column between the seafloor and the BSR in the western and eastern Nankai Trough. *Shyu et al.* [2006] assume lithostatic conditions and use a density of 1.7 g/cm³ for the sediment column above the BSR in the accretionary wedge off southwestern Taiwan.

[30] During the IODP Expeditions we obtained in situ borehole pressure while drilling, called the Annular Pressure (APRS-MWD) [*Tobin et al.*, 2009]. Although the measurements are made at the annulus near the drill bit and the data is influenced by the pump pressure, they basically remain near hydrostatic pres-

sure conditions except for the lower section (lower than 500 mbsf) at Site C0001.

[31] Thus we assume that the fore-arc slope studied here is in hydrostatic equilibrium. The pore pressure at the BSR horizon is simply calculated by integrating the weight of overburden seawater above BSR and using a seawater density of 1.024 g/cm³. We also estimated heat flow for a lithostatic condition using a density = 1.7 g/cm³ in the sediment column. The difference is 2–3 mW/m². These density differences lead to a systematic increase in heat flow of less than 1% [*He et al.*, 2007].

2.6. Seafloor Temperature

[32] Temperature at the seafloor is determined as 2°C, based on CTD measurements on the seafloor during submersible dive, or on mudline temperatures during IODP Expeditions 315 and 316. *H. Hamamoto et al.* (Heat flow distribution and thermal structure of the Nankai subduction zone off the Kii Peninsula, submitted to *Geochemistry, Geophysics, Geosystems*, 2011) pointed out that there is a significant amount of annual temperature variation with amplitude of 0.15°C near the seafloor in the Kumano Basin and the fore-arc slope region. Since the thermal skin depth for 1 year long temperature variation is ~10 m, temperature variation in the bottom water does not affect the heat flow estimation from depth to BSR.

2.7. Thermal Conductivity

[33] Since we do not have direct measurements of thermal conductivity in the ITZ, conductivity was estimated from the empirical relationship between P wave velocity (V_p) and thermal conductivity. A similar approach is made for IODP NanTroSEIZE drill sites below the depth of coring. The relationship between V_p and thermal conductivity for IODP NanTroSEIZE sites in the fore-arc slope area (Figure 7) is generally in good agreement with previous studies [e.g., *Horai*, 1981; *Martin et al.*, 2004], although the result from *Martin et al.* [2004] gives a slightly higher estimate of thermal conductivity (by 0.1 to 0.2 W m⁻¹ K⁻¹ at V_p = 2 km/s).

[34] We use the thermal conductivity value of 1.3 W m⁻¹ K⁻¹ in this study, although the uncertainties are as large as 0.1 W m⁻¹ K⁻¹, due to the discrepancies in measured versus model velocity and the scatter in thermal conductivity measurements.

[35] In summary, the heat flow estimated from BSR depth can have uncertainty of 20% or even more. The largest sources of uncertainties are temperature

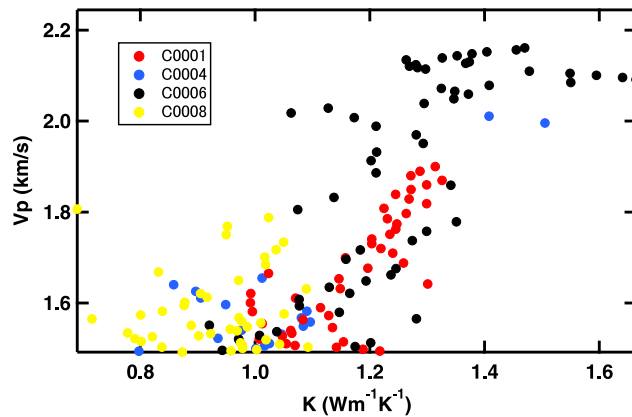


Figure 7. P wave velocity (V_p) versus thermal conductivity (K) at IODP Sites C0001 (red), C0004 (blue), C0006 (black) and C0008 (yellow). Thermal conductivities were measured for core samples using a needle probe or half-space method [Kinoshita *et al.*, 2009]. Interval velocity model was used to represent V_p at each site.

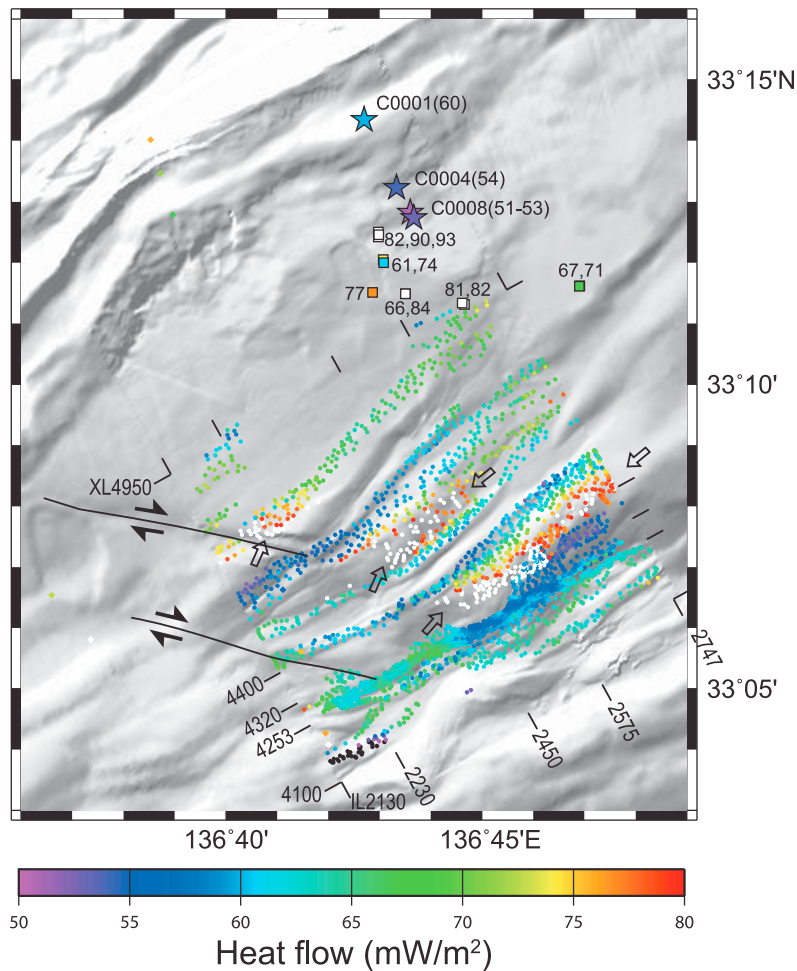


Figure 8. Heat flow distribution overlain above the bathymetry in the fore-arc slope region. Locations of Inline (IL) and crossline (XL) profiles in Figures 4 and 5 are shown. Dots are BSR-derived heat flow that were confidently picked from the PSDM profiles, squares are surface heat flow stations, and stars are NanTroSEIZE drill sites. Numbers attached to squares and stars indicate the heat flow values (mW/m^2) [Harris *et al.*, 2011; Hamamoto *et al.*, submitted manuscript, 2011]. Heat flow values are color coded, and those higher than 80 mW/m^2 and lower than 50 mW/m^2 are shown as white and black, respectively. High heat flow zones below the uplifted and eroded zones (see text for details) are indicated by open arrows.

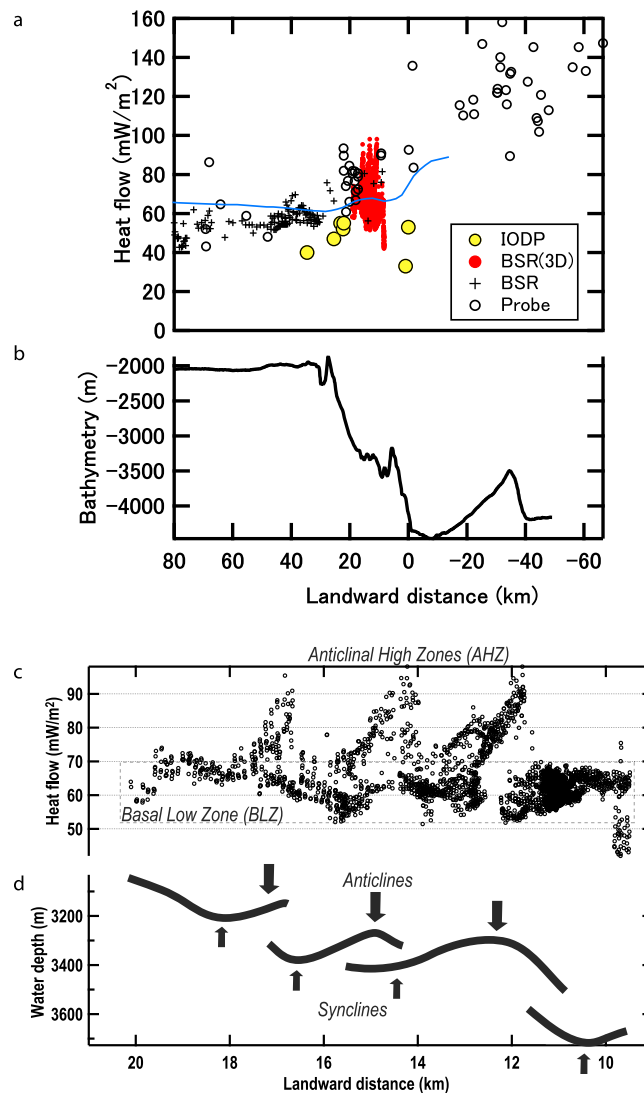


Figure 9. (a) Heat flow and (b) bathymetry cross section across the Nankai Trough off Kumano. Small open circles are surface heat flow measured by geothermal probes, large circles filled by yellow are heat flow determined in IODP holes [Harris *et al.*, 2011], black pluses are previous BSR-derived heat flow, and red dots are BSR-derived heat flow in this study. Solid curve is the numerically simulated heat flow (Hamamoto *et al.*, submitted manuscript, 2011). (c) BSR-derived heat flow and (d) smoothed bathymetry cross section versus landward distance from the deformation front (km) in the fore-arc slope region.

at BSR depth and thermal conductivity, but other sources can cause error of up to 10%.

3. Distribution of BSR and Apparent Heat Flow

[36] In the ITZ, we recognize three major ridges trending subparallel to the trench which are identified in Figure 4, between crosslines 4200–4400, 4500–4650 and 4750–4850. Moore *et al.* [2009] indicated that an apparent strike-slip fault offsets these ridges in the ITZ (Figure 8).

[37] Clear BSRs are typically associated with the landward slopes of anticlines below the ridges, parallel to the seafloor or obliquely crossing the stratigraphic reflectors upward toward the axis. One of the obliquely crossing BSRs (Figure 4; IL2575 between XL 4470–4380) seems to continue toward a stratum with stronger reflectivity below the anticline (XL 4360–4300). We suspect that this reflector coincides with the BSR, although we cannot discriminate the polarity change due to hydrate/gas transition with one resulting from lithological variation. Noteworthy is that these reflectors are significantly shallower than those in

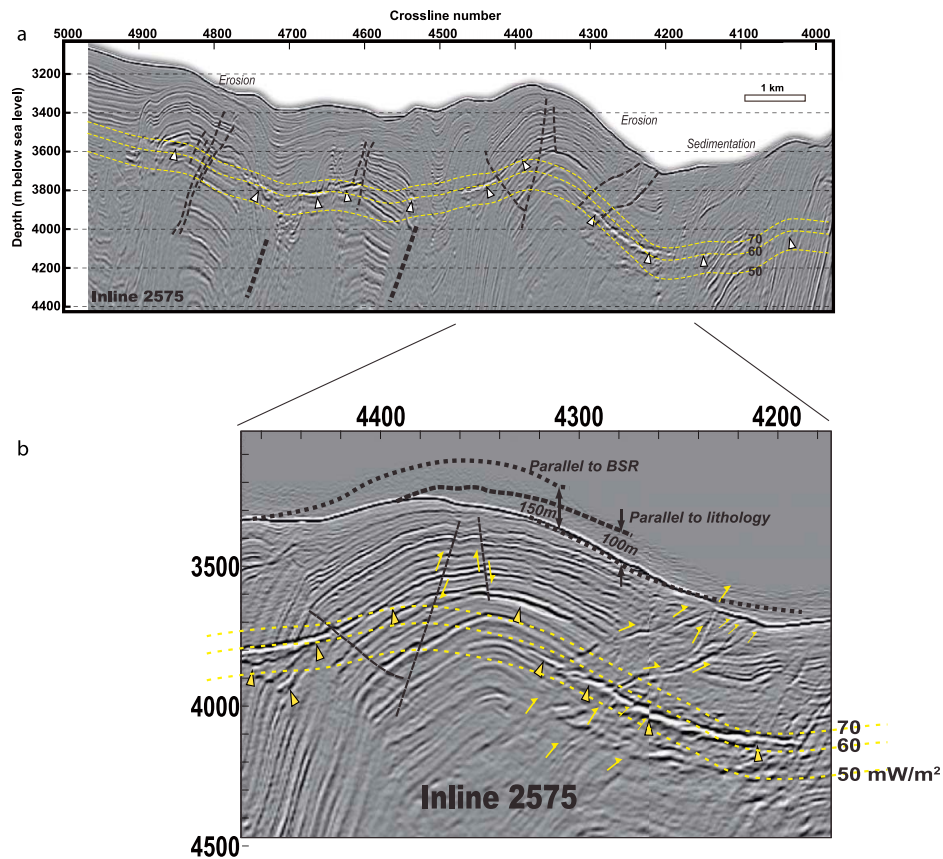


Figure 10. (a) PSDM cross section view of 3D seismic volumes along inline 2575, overlain by yellow dashed curves indicating the theoretical BSR depths distribution corresponding to uniform regional heat flow values 50, 60 and 70 mW/m^2 . BSR below anticlines are located shallower than the theoretical BSR of 70 mW/m^2 . (b) A blowup section around the overlapping BSR at crossline 4300. Dashed black lines are the inferred faults, and small yellow arrows suggest the orientation of fault displacement inferred from discontinuous horizons across them. Black dashed lines above the seafloor are the bathymetry inferred from BSR and lithological horizons.

the slope zones. Possible BSRs near the axis of anticlines seem to continue seaward, until they are truncated in the slope, and appear again at a depth similar to one on the landward slope. For the convenience of discussion here, we designate the shallow BSR below the ridge axes “Anticlinal High Zone (AHZ),” and designate the other BSR “Basal Low Zone (BLZ).”

[38] On inlines 2260, 2450 and 2575, some AHZ and BLZ slightly overlap between crosslines 4200 and 4300. On inline 2747 we can recognize the double BSRs between crosslines 4350 and 4500 (Figure 4e). A series of thrust faults cross between AHZ and BLZ, which would give the impression that the thrust faulting resulted in the offset between AHZ and BLZ in the seaward slope. BSRs are not seen below synclines.

[39] BSRs can be identified only in the ITZ and no BSRs are visible either around the megasplay fault

or the accretionary toe zones (Figure 8). In plan view, high heat flow at AHZ extends along the ridges and is truncated by the strike-slip fault.

[40] A heat flow cross section projected across the accretionary prism (Figures 9a and 9b) shows that the BSR-derived heat flow is generally consistent with the heat flow trend which gradually decreases landward, from 120 to 140 mW/m^2 in the Shikoku Basin to $\sim 55 \text{ mW/m}^2$ in the Kumano Fore-arc Basin. Note that the heat flow measured using geothermal probes is susceptible to be modified by bottom water temperature variations and sediment/erosion effects. Furthermore, some of them are the projected values and along strike variability may be large.

[41] In closer view, the BSR-derived heat flow is apparently classified into two populations, 55–65 mW/m^2 at BLZ and 70–90 mW/m^2 at AHZ (Figures 9c and 9d). This is demonstrated more clearly by comparing the observed BSR with

the theoretical BSR, estimated using a method similar to that used to calculate heat flow in the previous section, for a given water depth and a basal heat flow. An example of the simulated BSRs (Figure 10, yellow dashed curves) for three basal heat flow values of 50, 60 and 70 mW/m² shows that observed BSRs in the BLZ basically lie between simulated BSRs corresponding to 60 and 70 mW/m². BSRs below anticlines (AHZ) are located shallower than the simulated BSR corresponding to 70 mW/m².

[42] Heat flow values in BLZ are slightly lower than values obtained from probe measurements in the slope region (60–90 mW/m², see Figures 9a and 9b). On the other hand, our new heat flow values are generally in good agreement with those obtained at IODP drill sites in the fore-arc slope region (51–60 mW/m²) [*Expedition 316 Scientists*, 2009a, 2009b, 2009c, 2009d; *Harris et al.*, 2011]. The maximum depth for in situ temperature measurements is 250 m below the seafloor, almost equivalent to the depth of BSRs (300–500 m below the seafloor).

4. Shallow BSR Anomaly Below Anticlines

[43] Figure 10 shows that the discontinuity in the BSRs between AHZ and BLZ occurs across the thrust faults forming the ITZ. The amount of discontinuity in the BSRs below the seaward slopes of anticlines reaches as much as 200 m at water depths of ~3500 m. The apparent heat flow values suggest that the BSR at AHZ is shallower than thermally equilibrated BSR depth.

[44] Changes in the bottom water temperature or in the sea level are ruled out as a mechanism of such discontinuity, simply because they should affect the whole region. Fluid migration along the fault is reported as a thermally uplifted BSR near a thrust in the Cascadia accretionary prism [*Shipboard Scientific Party*, 1994]. In this region, however, we find no clear evidence for fluid flow at anticlines, such as cold seeps and biological communities on the seafloor, or seismic evidence for shallowing BSR toward the fault.

[45] Thrust faulting will be followed by uplift and erosion on the hanging wall side of the thrust, and by the subsidence and sedimentation on the footwall side. The uplift can cause upward migration of BGHS because the pressure at the BSR is reduced. The amount of such migration, as derived from the

P-T phase diagram, is only 3–4% of the total uplift at a water depth of ~2500 m and at the basal heat flow of 60 mW/m². In other words, if a block is uplifted by 100 m, the BGHS depth below the seafloor becomes shallower by only 3–4 m, which is much smaller than the observed discontinuity.

[46] Thus we suggest that the shallow BSR below anticlines is primarily a result of the erosion caused by the uplift along the anticlines. *Hornbach et al.* [2008] demonstrated that the gas hydrate stability boundary significantly varies in areas of high sedimentation or erosion. These activities have to be considered as time-dependent phenomena.

5. BSR Adjustment Following the Uplift and Erosion

5.1. Model

[47] In the ITZ, a series of thrust faults cause uplift on the landward side and subsidence on the seaward side (Figure 11). For an instantaneous fault offset, the BSR horizon should also be geometrically shifted across the fault plane.

[48] On the hanging wall side, the BSR horizon becomes shallower instantaneously by the same amount as the fault offset (Figure 11b). Likewise on the footwall side, the formation will subside and sediment will fill the trough. The pressure effect on BGHS migration is small and ignored.

[49] The uplift will be followed by erosion (Figure 11c), as seen in seismic profiles (e.g., Figure 10). We cannot determine the exact time and amount of erosion directly. But if we assume that the uplifted sediment layers remain parallel through faulting, extrapolation of the landward slope layer (which we assume is not eroded) parallel toward the seaward side provides a rough estimate of erosion amount as ~100 m (Figure 10b). Note that erosion does not affect the pressure at the BSR, because we assume here a hydrostatic state down to BSR depth. Therefore the model should only have to deal with thermal diffusion process.

[50] The geothermal field around the fault will reequilibrate to this new geometry, and the BGHS on the hanging wall side should gradually deepen following the change in temperature. The time constant for the adjustment depends on thermal diffusivity and the amount of adjustment. More importantly, the latent heat of fusion, absorbed or released for phase transition between hydrate and gas, should significantly affect the amount of phase

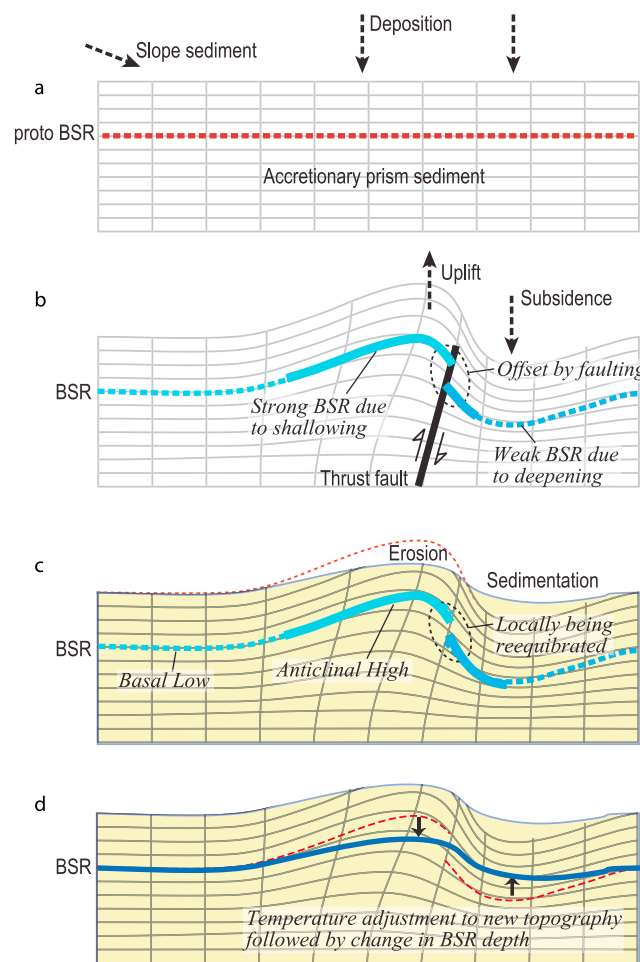


Figure 11. Schematics explaining relationship between tectonic activity and transient BSR. (a) Depositional phase (>1 Ma). (b) Faulting (repeated; <1 Ma to ~10 kyr). (c) Erosion/sedimentation following the faulting occurring simultaneously with faulting. Adjustment of thermal field and relocating BSR depth are ongoing to present. (d) Thermal equilibrium that is not yet achieved.

boundary displacement [Golmshtok and Soloviev, 2006] and reduce the thermal adjustment rate [Kinoshita et al., 1998; Sultan et al., 2004]. Thus, the BSR across the fault zone remains discontinuous for a while (Figure 11c) before it is readjusted and continuous again (Figure 11d).

5.2. One-Dimensional Numerical Calculation

[51] We construct a one-dimensional time-dependent numerical model in order to simulate the temporal change in the depth of BGHS after sudden uplift and erosion on the hanging wall.

[52] The effect of latent heat across the gas/hydrate phase transition is incorporated in the model. Sultan et al. [2004] introduced an enthalpy form of the conservation of energy in order to simplify the numerical treatment. We took a similar approach

but in the temperature form. In each 1-D grid we define a heat buffer with its size equal to the latent heat for gas/hydrate transition. This buffer is empty for hydrate and full for the gas. The new temperature at each grid (depth) T is calculated using an ordinary thermal conduction equation, and is adjusted according to the state of the buffer. While the buffer is partially filled (i.e., this grid is in the phase transition state), external thermal energy is exchanged only with this buffer, and T is fixed to be the phase transition temperature at that depth (T_H), until this buffer becomes full or empty.

[53] Parameters used in the simulation are listed in Table 1. We set the latent heat of hydrate dissociation/formation as 500kJ/kg [Ruppel, 1997]. We have no data on the hydrate saturation and porosity in the ITZ, thus calculations were made on three different values for total hydrate weight content, 0, 10 and 20%. Thermal diffusivity is set as $3.3 \cdot 10^{-7} \text{ m}^2/\text{s}$.

Table 1. Parameters Used for the Numerical Simulation

Parameter	Symbol (Unit)	Value	Comments
Hydrate volume fraction	(-)	0/0.1/0.2	Three cases
Latent heat	(Jkg ⁻¹)	5 * 10 ⁵	Ruppel [1997]
Basal heat flux	(mWm ⁻²)	70	
Thermal conductivity	λ (Wm ⁻¹ K ⁻¹)	1.3	estimated from IODP data
Seawater density	ρ (kgm ⁻³)	1024	
Heat capacity	c (Jkg ⁻¹ K ⁻¹)	4 * 10 ³	
Thermal diffusivity	(m ² s ⁻¹)	3.3 * 10 ⁻⁷ = λ / (ρ c)	
Water depth	(m)	2600	
Initial depth of BGHS	(m)	2950	estimated from P-T diagram
Total uplift (=erosion)	(m)	100	at once/10 m at every 100 y/10 m at every 1000 y
Grid spacing	(m)	1 or 10	fine mesh around BGHS
Time increment	(s)	10 ⁶	

[54] Water depth before erosion is set at 2600 m, and the total amount of uplift (= erosion) is given as 100 m. The change should be an integration of multiple events with various amplitude (one to a few tens of meters), each of which has occurred repeatedly in different times. Thus we calculated three scenarios; a single event with 100 m offset, 10 events with 10 m offset at every 100 years and at every 1000 years.

[55] Temperature gradient is assumed as 60 mK/m, resulting in the BSR depth of ~300 m below the seafloor.

5.3. Results

[56] The time variation of the BGHS depth after the onset of uplift and erosion is shown in Figure 12. Dependence of the thermal equilibration time con-

stant on hydrate inclusion is also shown. For a single event scenario with 100 m uplift/erosion, the time to recover 50% of the initial depth shift is 7,000 years for 0% total hydrate fraction, 12,000 years (10%), and 16,000 years (20%). For multiple events scenario with 10% hydrate fraction, the time constant is 12,000 for the 100 year interval case and 20,000 years for the 1,000 year interval case. Both cases give a time constant basically similar to that for a single event scenario. Thus in either scenario, the uplift and erosion should have occurred within ~10,000 years before present, if the observed BSR corresponds to the *present* P-T condition.

[57] On the other hand, if the tectonic events have occurred earlier than ~10,000 years, the shallow BSRs in the AHZ cannot correspond to the present BGHS. Similarly, multiple uplifts would be difficult to maintain the original thermal state if the event

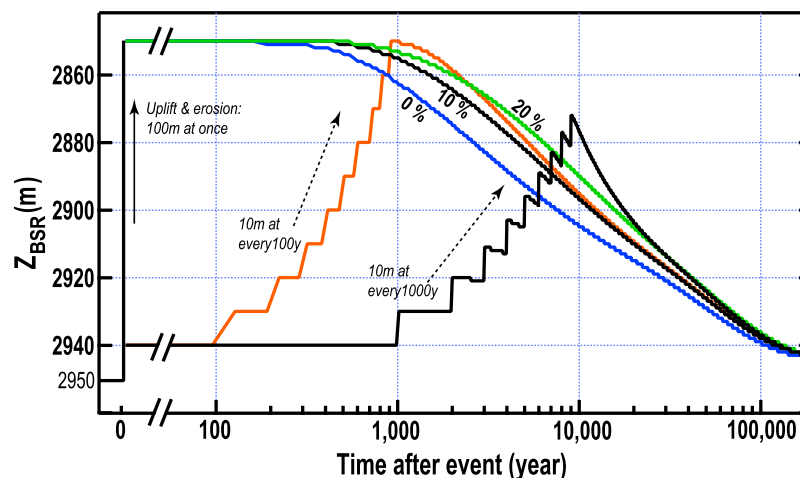


Figure 12. Transient effect of sudden uplift followed by erosion (by 100 m) on the depth change in BSR. Numerical simulation of 1D time-dependent thermal conduction model, taking the latent heat of hydrate formation/dissociation into account. The original BSR depth is assumed as 2950 m. Smooth curves, single event with 100 m offset, with the total hydrate weight content of 0, 10 and 20%; stepwise curves, 10 events with 10 m offset at every 100 years (red), at every 1000 years (black).

interval is longer than ~1,000 years. In such cases, the shallow BSR anomaly would be a remnant BSR.

6. Discussion

[58] Ages of slope sediment and the accretionary prism near the megasplay fault zone were revealed from the paleontological and paleomagnetic analyses at Sites C0004 and C0008 [*Expedition 316 Scientists*, 2009a, 2009d]. The accretionary prism at Site C0008 was formed at a frontal prism toe position sometime between 2.87 and 1.95 Ma [*Strasser et al.*, 2009]. Near the present accretionary toe position at Sites C0006/C0007, ages of accreted sediments are 0.4–1 Ma [*Expedition 316 Scientists*, 2009b, 2009c]. By interpolating results from Sites C0004/C0008 and Sites C0006/C0007, the depositional age of the accretionary prism at ITZ should be between 1Ma and 2Ma (Figure 11a).

[59] *Strasser et al.* [2009] indicated that the activity of the megasplay thrust crossing Site C0004 decreased during 1.8–1.55Ma, and suggested that the plate convergence was more efficiently accommodated by forward propagation of the deformation front, creating an in-sequence frontal imbrication. We infer that the thrusts in the ITZ was originally formed between 1.8 and 1.55 Ma.

[60] The erosional feature on the seaward slope of the anticline (Figure 10) indicates that the surface sediment erosion has been occurring up to the present. Also, as shown in Figure 10b, some faults offset the sediment near the seafloor, and a series of small offsets (10–20 m) across the thrust faults are identified (yellow arrows between crosslines 4200 and 4300). In addition to the numerical simulation in this study, these lines of evidence strongly suggest that the ridges in the ITZ should have been uplifting since 10 kyr B.P. In this case, the thermal regime and the BSR depth in the AHZ have not yet equilibrated after the uplift, resulting in anomalously shallow BSR depth.

[61] It does not, however, preclude the possibility that the shallow BSR below anticlines is a remnant BSR. If a remnant BSR is caused by the past uplift/erosion before 10 kyr, the present BGHS should be located deeper than BSR; it would either be seen as a deeper part of the overlapping/double BSR, or it has not yet established a strong enough impedance contrast. The upper BSR could be the base of a hydrate cemented layer within the GHSZ, below which the hydrate has not been formed dense enough to eliminate the impedance contrast.

[62] We infer that the primary mechanism for generating the double/overlapping BSR here would be the erosion due to uplift. Other mechanisms, such as increase in the bottom water temperature, sea level rise or tectonic uplift, are suggested for the double BSR in the eastern Nankai Trough [*Foucher et al.*, 2002; *Matsumoto et al.*, 2004; *Golmshtok and Soloviev*, 2006; *Takeuchi and Matsumoto*, 2009]. However, they do not apply in this area due to the same reason described in section 4 in this paper.

[63] Based on the drilling results and observations from 3D seismic profiles at the toe of Nankai accretionary prism, *Screaton et al.* [2009b] suggest that the frontal thrust system would have accommodated at least ~13 to 34% of the total plate convergence since the time between 0.436 and 0.78 Ma. Horizontal shortening at ITZ may be ~300 m as estimated from the vertical uplift (~100 m) and the dip angle of the thrust (15–20°). Although we have no independent age constraints in the ITZ, if the shortening has occurred in the recent 10 kyr the convergent rate would be ~30 m/kyr. It is much larger than the recent horizontal shortening rate of ~1 m/kyr at the megasplay fault [*Kimura et al.*, 2011], and shares a significant portion of the total plate convergent rate (~50 m/kyr).

[64] We cannot exclude the possibility that the shallow BSR below anticlines is a remnant BSR generated by past uplift/erosion before 10 kyr. Nevertheless, the lines presented in Figure 4 (notably inline 2180 and inline 2575) provide compelling evidence that the thrust faults offset the seafloor and, therefore are active.

[65] As pointed out earlier, the zones of anomalously shallow BSR (AHZ) are only found north of a scarp interpreted as a strike-slip fault. Furthermore, the apparent heat flow anomalies, as well as the evidence for active thrusting in the seismic profiles appear to fade northeastward along the thrust, away from the intersection with the strike slip fault. There is little doubt that, locally, the ITZ shares a significant amount of the total plate convergent rate with the frontal region. How, and on which structures, the motion is transferred laterally remains to be understood.

7. Conclusions

[66] BSR-derived heat flow values are added in the fore-arc slope region where surface heat flow data were difficult to obtain because of rough topography and noise from bottom water temperature variation. The base value, 55–65 mW/m², is generally con-

sistent with heat flow obtained at IODP drillsites. An anomalously shallow BSR below the axes of three anticlines in the imbricate thrust zone produce an apparent high heat flow anomaly of 70–90 mW/m². Such BSRs are terminated or discontinuous across the thrust fault zone. We propose that the anomalously shallow BSR on the forelimb of thrust anticlines and the BSR discontinuity across these fault zones are primarily caused by active thrusting followed by erosion, occurring over the last 10 kyr or more.

[67] Thrusting within the ITZ represents, at least locally, a significant portion of the plate convergence motion. This shows that the internal deformation within an accretionary wedge should not be neglected, even at a time when no frontal accretion is occurring.

Acknowledgments

[68] The authors are grateful to Robert N. Harris for providing data in advance of publication. The manuscript was greatly improved by thorough reviews by George Spence, Ingo Grevermeyer and the Associate Editor Pierre Henry. Funding for this study was supported by the Grant-in-Aid for Scientific Research on Innovative Areas (21107006) and Grant-in-Aid for Creative Scientific Research (19GS0211) and the U.S. National Science Foundation (OCE-0451790). Borehole data were provided by the Integrated Ocean Drilling Program (IODP). We are grateful to the crew and technicians of D/V Chikyu and Center for Deep Earth Exploration of Japan Agency for Marine-Earth Science and technology for the successful operations during IODP Expeditions 314, 315 and 316. SOEST contribution 8259.

References

- Ashi, J., H. Tokuyama, and A. Taira (2002), Distribution of methane hydrate BSRs and its implication for the prism growth in the Nankai Trough, *Mar. Geol.*, *187*, 177–191, doi:10.1016/S0025-3227(02)00265-7.
- Ashi, J., S. Lallemand, H. Masago, and the Expedition 315 Scientists (2009), Expedition 315 summary, *Proc. Integrated Ocean Drill. Program*, *314/315/316*, 1–57, doi:10.2204/iodp.proc.314315316.121.2009.
- Bangs, N. L., M. J. Hornbach, G. F. Moore, and J.-O. Park (2010), Massive methane release triggered by seafloor erosion offshore southwestern Japan, *Geology*, *38*, 1019–1022, doi:10.1130/G31491.1.
- Blackwell, D. D., J. L. Steele, and C. A. Brott (1980), The terrain effect on terrestrial heat flow, *J. Geophys. Res.*, *85*(B9), 4757–4772, doi:10.1029/JB085iB09p04757.
- Davie, M. K., and B. A. Buffet (2001), A numerical model for the formation of gas hydrate below the seafloor, *J. Geophys. Res.*, *106*, 497–514, doi:10.1029/2000JB900363.
- Davis, E. E., H. Villinger, R. D. MacDonald, R. D. Meldrum, and J. Grigel (1997), A robust rapid-response probe for measuring bottom-hole temperatures in deep-ocean boreholes, *Mar. Geophys. Res.*, *19*, 267–281, doi:10.1023/A:1004292930361.
- DeMets, C., R. G. Gordon, and D. F. Argus (2010), Geologically current plate motions, *Geophys. J. Int.*, *181*, 1–80, doi:10.1111/j.1365-246X.2009.04491.x.
- Dickens, G. R., and M. S. Quinby-Hunt (1994), Methane hydrate stability in seawater, *Geophys. Res. Lett.*, *21*, 2115–2118, doi:10.1029/94GL01858.
- Expedition 316 Scientists (2009a), Expedition 316 Site C0004, *Proc. Integrated Ocean Drill. Program*, *314/315/316*, 1–107, doi:10.2204/iodp.proc.314315316.133.2009.
- Expedition 316 Scientists (2009b), Expedition 316 Site C0006, *Proc. Integrated Ocean Drill. Program*, *314/315/316*, 1–124, doi:10.2204/iodp.proc.314315316.134.2009.
- Expedition 316 Scientists (2009c), Expedition 316 Site C0007, *Proc. Integrated Ocean Drill. Program*, *314/315/316*, 1–110, doi:10.2204/iodp.proc.314315316.135.2009.
- Expedition 316 Scientists (2009d), Expedition 316 Site C0008, *Proc. Integrated Ocean Drill. Program*, *314/315/316*, 1–107, doi:10.2204/iodp.proc.314315316.136.2009.
- Foucher, J.-P., H. Nouzé, and P. Henry (2002), Observation and tentative interpretation of a double BSR on the Nankai slope, *Mar. Geol.*, *187*, 161–175, doi:10.1016/S0025-3227(02)00264-5.
- Golmshtok, A. Y., and V. A. Soloviev (2006), Some remarks on the thermal nature of the double BSR, *Mar. Geol.*, *229*, 187–198, doi:10.1016/j.margeo.2006.03.004.
- Grevermeyer, I., and H. Villinger (2001), Gas hydrate stability and the assessment of heat flow through continental margins, *Geophys. J. Int.*, *145*, 647–660, doi:10.1046/j.0956-540x.2001.01404.x.
- Haacke, R. R., G. K. Westbrook, and R. D. Hyndman (2007), Gas hydrate, fluid flow and free gas: Formation of the bottom-simulating reflector, *Earth Planet. Sci. Lett.*, *261*, 407–420, doi:10.1016/j.epsl.2007.07.008.
- Harris, R. N., F. Schmidt-Schierhorn, and G. Spinelli (2011), Heat flow along the NanTroSEIZE transect: Results from IODP expeditions 315 and 316 offshore the Kii Peninsula, Japan, *Geochem. Geophys. Geosyst.*, *12*, Q0AD16, doi:10.1029/2011GC003593.
- He, T., G. D. Spence, M. Riedel, R. D. Hyndman, and N. R. Chapman (2007), Fluid flow and origin of a carbonate mound offshore Vancouver Island: Seismic and heat flow constraints, *Mar. Geol.*, *239*, 83–98, doi:10.1016/j.margeo.2007.01.002.
- Henry, P., M. Thomas, and M. B. Clenell (1999), Formation of natural hydrates in marine sediments: 2. Thermodynamic calculations of stability conditions in porous sediments, *J. Geophys. Res.*, *104*, 23,005–23,022, doi:10.1029/1999JB900167.
- Holbrook, W. S., H. Hoskins, W. T. Wood, R. A. Stephen, D. Lizzaralde, and the Leg 164 Science Party (1996), Methane gas-hydrate and free gas on the Blake Ridge from vertical seismic profiling, *Science*, *273*, 1840–1843, doi:10.1126/science.273.5283.1840.
- Horai, K. (1981), Thermal conductivity of sediments and igneous rocks recovered during Deep Sea Drilling Project Leg 60, *Initial Rep. Deep Sea Drill. Proj.*, *60*, 807–834.
- Hornbach, M. J., D. M. Saffer, W. S. Holbrook, H. J. A. Van Avendonk, and A. R. Gorman (2008), Three-dimensional seismic imaging of the Blake Ridge methane hydrate province: Evidence for large, concentrated zones of gas hydrate and morphologically driven advection, *J. Geophys. Res.*, *113*, B07101, doi:10.1029/2007JB005392.
- Hyndman, R. D., and E. E. Davis (1992), A mechanism for the formation of methane hydrate and seafloor bottom-simulating-reflectors by vertical fluid expulsion, *J. Geophys. Res.*, *97*(B5), 7025–7041, doi:10.1029/91JB03061.

- Hyndman, R. D., E. E. Davis, and J. A. Wright (1979), The measurement of marine geothermal heat flow by a multipenetration probe with digital acoustic telemetry and in-situ thermal conductivity, *Mar. Geophys. Res.*, *4*, 181–205, doi:10.1007/BF00286404.
- Hyndman, R. D., J. P. Foucher, M. Yamano, A. Fisher, and Scientific Team of Ocean Drilling Program Leg 131 (1992), Deep sea bottom-simulating-reflectors: Calibration of the base of the hydrate stability field as used for heat flow estimates, *Earth Planet. Sci. Lett.*, *109*, 289–301, doi:10.1016/0012-821X(92)90093-B.
- Kimura, G., G. F. Moore, M. Strasser, E. Sreaton, D. Curewitz, C. Streiff, and H. Tobin (2011), Spatial and temporal evolution of the megasplay fault in the Nankai Trough, *Geochem. Geophys. Geosyst.*, *12*, Q0A008, doi:10.1029/2010GC003335.
- Kinoshita, M., Y. Nakano, S. Goto, and J. Ashi (1998), Effect of the latent heat on the gas-hydrate /gas phase boundary depth due to faulting [in Japanese with English abstract], *Bull. Earthquake Res. Inst.*, *73*, 305–317.
- Kinoshita, M., T. Kanamatsu, K. Kawamura, T. Shibata, H. Hamamoto, and K. Fujino (2008), Heat flow distribution on the floor of Nankai Trough off Kumano and implications for the geothermal regime of subducting sediments, *JAMSTEC Rep. Res. Dev.*, *8*, 13–28.
- Kinoshita, M., H. Tobin, J. Ashi, G. Kimura, S. Lallemand, E. J. Sreaton, D. Curewitz, H. Masago, K. T. Moe, and the Expedition 314/315/316 Scientists (2009), *Proceedings of the Integrated Ocean Drilling Program*, vol. 314/315/316, Integrated Ocean Drill. Program, College Station, Tex., doi:10.2204/iodp.proc.314315316.2009.
- Kvenvolden, K. A. (1993), Gas hydrates—Geological perspective and global change, *Rev. Geophys.*, *31*, 173–187, doi:10.1029/93RG00268.
- Maekawa, T., S. Itoh, S. Sakata, S. Igari, and N. Imai (1995), Pressure and temperature conditions for methane hydrate dissociation in sodium chloride solutions, *Geochem. J.*, *29*, 325–329.
- Martin, V., P. Henry, H. Nouze, M. Noble, J. Ashi, and G. Pascal (2004), Erosion and sedimentation as processes controlling the BSR-derived heat flow on the Eastern Nankai margin, *Earth Planet. Sci. Lett.*, *222*(1), 131–144, doi:10.1016/j.epsl.2004.02.020.
- Matsumoto, R., H. Tomaru, and H. Lu (2004), Detection and evaluation of gas hydrates in the eastern Nankai Trough by geochemical and geophysical methods, *Resour. Geol.*, *54*, 53–67, doi:10.1111/j.1751-3928.2004.tb00187.x.
- Moore, G. F., N. L. Bangs, A. Taira, S. Kuramoto, E. Pangborn, and H. J. Tobin (2007), Three-dimensional splay fault geometry and implications for tsunami generation, *Science*, *318*(5853), 1128–1131, doi:10.1126/science.1147195.
- Moore, G. F., et al. (2009), Structural and seismic stratigraphic framework of the NanTroSEIZE Stage 1 transect, *Proc. Integrated Ocean Drill. Program*, *314/315/316*, 1–46, doi:10.2204/iodp.proc.314315316.102.2009.
- Okino, K., Y. Shimakawa, and S. Nagaoka (1994), Evolution of the Shikoku Basin, *J. Geomagn. Geoelectr.*, *46*, 463–479, doi:10.5636/jgg.46.463.
- Park, J.-O., T. Tsuru, S. Kodaira, P. R. Cummins, and Y. Kaneda (2002), Splay fault branching along the Nankai subduction zone, *Science*, *297*(5584), 1157–1160, doi:10.1126/science.1074111.
- Park, J.-O., G. Fujie, L. Wijerathne, T. Hori, S. Kodaira, Y. Fukao, G. F. Moore, N. L. Bangs, S. Kuramoto, and A. Taira (2010), A low-velocity zone with weak reflectivity along the Nankai subduction zone, *Geology*, *38*, 283–286, doi:10.1130/G30205.1.
- Ruppel, C. (1997), Anomalous cold temperature observed at the base of the gas hydrate stability zone on the U.S. Atlantic passive margin, *Geology*, *25*, 699–702, doi:10.1130/0091-7613(1997)025<0699:ACTOAT>2.3.CO;2.
- Sreaton, E. J., G. Kimura, D. Curewitz, and the Expedition 316 Scientists (2009a), Expedition 316 summary, *Proc. Integrated Ocean Drill. Program*, *314/315/316*, 1–73, doi:10.2204/iodp.proc.314315316.131.2009.
- Sreaton, E., et al. (2009b), Interactions between deformation and fluids in the frontal thrust region of the NanTroSEIZE transect offshore the Kii Peninsula, Japan: Results from IODP Expedition 316 Sites C0006 and C0007, *Geochem. Geophys. Geosyst.*, *10*, Q0AD01, doi:10.1029/2009GC002713.
- Shipboard Scientific Party (1994), Site 892, *Proc. Ocean Drill. Program Initial Rep.*, *146*, part 1, 301–378, doi:10.2973/odp.proc.ir.146-1.010.1994.
- Shibley, T. H., M. H. Houston, R. T. Buffler, F. J. Shuab, K. J. McMillen, J. W. Ladd, and U. J. L. Worzel (1979), Seismic reflection evidence for the widespread occurrence of possible gas-hydrate horizons on continental slopes and rises, *Am. Assoc. Pet. Geol. Bull.*, *63*, 2204–2213.
- Shyu, C.-T., Y.-J. Chen, S.-T. Chiang, and C.-S. Liu (2006), Heat flow measurements over bottom simulating reflectors, offshore southwestern Taiwan, *Terr. Atmos. Oceanic Sci.*, *17*, 845–869.
- Singh, S. C., T. A. Minshull, and G. D. Spence (1993), Velocity structure of a gas hydrate reflector, *Science*, *260*, 204–207, doi:10.1126/science.260.5105.204.
- Strasser, M., et al. (2009), Origin and evolution of a splay fault in the Nankai accretionary wedge, *Nat. Geosci.*, *2*, 648–652, doi:10.1038/ngeo609.
- Strasser, M., G. F. Moore, G. Kimura, A. J. Kopf, M. B. Underwood, J. Guo, and E. J. Sreaton (2011), Slumping and mass-movement deposition in the Nankai forearc: Evidence from IODP drilling and 3-D reflection seismic data, *Geochem. Geophys. Geosyst.*, *12*, Q0AD13, doi:10.1029/2010GC003431.
- Sultan, N., J. P. Foucher, P. Cochonat, T. Tonnerre, J. F. Bourillet, H. Ondreas, E. Cauquil, and D. Grauls (2004), Dynamics of gas hydrate: Case of the Congo continental slope, *Mar. Geol.*, *206*, 1–18, doi:10.1016/j.margeo.2004.03.005.
- Takeuchi, R., and R. Matsumoto (2009), Geological and geochemical constraints on the process of gas hydrate formation and accumulation in the Eastern Nankai Trough, off central Japan [in Japanese with English abstract], *J. Geogr.*, *118*, 793–813, doi:10.5026/jgeography.118.793.
- Tobin, H. J., and M. Kinoshita (2006), NanTroSEIZE: The IODP Nankai Trough Seismogenic Zone Experiment, *Sci. Drill.*, *2*, 23–27, doi:10.2204/iodp.sd.2.06.2006.
- Tobin, H., M. Kinoshita, K. T. Moe, and the Expedition 314 Scientists (2009), Expedition 314 summary, *Proc. Integrated Ocean Drill. Program*, *314/315/316*, 1–42, doi:10.2204/iodp.proc.314315316.111.2009.
- White, R. S. (1979), Gas hydrate layers trapping free gas in the Gulf of Oman, *Earth Planet. Sci. Lett.*, *42*, 114–120, doi:10.1016/0012-821X(79)90196-1.
- Yamano, M., S. Uyeda, Y. Aoki, and T. H. Shipley (1982), Estimates of heat flow derived from gas hydrates, *Geology*, *10*(7), 339–343, doi:10.1130/0091-7613(1982)10<339:EOHFDf>2.0.CO;2.